APPLIED SCIENCES AND ENGINEERING

Printable elastomeric electrodes with sweat-enhanced conductivity for wearables

Jian Lv[1†], Gurunathan Thangavel[1†], Yi Li[1,2], Jiaqing Xiong[1‡], Dace Gao[1], Jinghao Ciou[1], Matthew Wei Ming Tan[1], Izzat Aziz[1], Shaohua Chen[1], Juntong Chen[1], Xinran Zhou[1], Wei Church Poh[1], Pooi See Lee[1]*

We rationally synthesized the thermoplastic and hydrophilic poly(urethane-acrylate) (HPUA) binder for a type of printable and stretchable Ag flakes–HPUA (Ag-HPUA) electrodes in which the conductivity can be enhanced by human sweat. In the presence of human sweat, the synergistic effect of Cl^- and lactic acid enables the partial removal of insulating surfactant on silver flakes and facilitates sintering of the exposed silver flakes, thus the resistance of Ag-HPUA electrodes can be notably reduced in both relaxed and stretched state. The on-body data show that the resistance of one electrode has been decreased from 3.02 to 0.62 ohm during the subject's 27-min sweating activity. A stretchable textile sweat-activated battery using Ag-HPUA electrodes as current collectors and human sweat as the electrolyte was constructed for wearable electronics. The enhanced conductivity of the wearable wiring electrode from the reaction with sweat would provide meritorious insight into the design of wearable devices.

INTRODUCTION

In the past decade, innovations in functional materials, mechanics, and device design have stimulated the surging development of wearable devices including sensing, signal transmission, and power sources (*1*–*5*). The key components in wearable devices are the flexible and soft functional electrodes and conductive wiring (*6*, *7*). The interaction between wearable electrodes and body motion, body heat, or biofluids can be applied to realize real-time physiological signal sensing (*8*), human-machine interactions (*9*), drug delivery (*10*), or bioenergy harvesting (*11*, *12*). The materials design and interaction mechanism of wearable devices with the human body are vital for the successful realization for specific applications, which would open up a previously unknown era for the design of wearable devices. However, most of the research focuses on the versatile design of the functional electrodes, and the effect of biofluids on the conductive wiring has rarely been studied.

Human sweat is one of the most available biofluids that have been applied in the fabrication of noninvasive biosensors for continuous monitoring of physiological information (*13*–*15*). In addition, biocompatible and safe wearable biofuel cells (*16*, *17*), supercapacitors (*18*), and batteries (*19*) that used human sweat as electrolytes have been fabricated as power sources for wearable sensors. Sweat containing lactic acid and glucose and ions (such as Na^+ and Cl^-) enables the realization of wearable biofuel cells, supercapacitors, and batteries to function well as their regular counterparts. Conductive and stretchable wiring plays a key role in the design and fabrication of stretchable devices. Among various flexible/stretchable conductors, nano/micro Ag flakes–based electrodes have been widely used in conductive textiles, printed flexible/stretchable electronics, and microelectronic packaging for their high conductivity, stability, and scalable manufacturability (*20*–*22*). Typically, the effect of sweat on the Ag electrode has always been considered a deteriorating effect for electrode's conductivity because of the enhanced corrosion behavior of bulk metals in the presence of saline solution (*23*). This stereotype has impeded the investigations on the interaction between metal-based flexible/stretchable electrodes with sweat. Until now, no reported works have shown that the interaction with sweat biofluid has a potentially positive influence on stretchable electrodes.

Here, we demonstrate the first example of stretchable Ag electrodes in which the conductivity can be enhanced by human sweating behavior. The stretchable electrodes were fabricated by directly printing the ink composing of conductive filler Ag flakes and rationally designed elastic binder hydrophilic poly(urethane-acrylate) (HPUA) on hydrophilic textiles. The high stretchability and good hydrophilicity of the HPUA elastic binder are ascribed to the presence of rationally controlled hard-soft domains and the existence of urethane-acrylate (C═C) groups, respectively. In the presence of sweat, the Cl^- and the acidic environment work synergistically to remove the surfactant of the Ag flakes and increase the connections of adjacent flakes on printed electrodes, which can reduce the resistance of electrodes in both relaxed and stretched states, as shown in Fig. 1A. When one electrode was mounted on a subject's arm with sweat, its resistance could be decreased from 3.02 to 0.62 ohm, showing the positive effect of sweating on wiring electrodes. As an example to show the application of our sweat-enhanced stretchable electrodes, a kind of stretchable safe zinc battery using human sweat as the electrolyte and Ag-HPUA electrodes as the current collector was printed on textiles to serve as the wearable power source that can function under 50% strain.

RESULTS

Figure 1B shows the formulation of the ink for Ag-HPUA in which the Ag flakes and HPUA served as the conductive fillers and elastic binder, respectively. Ag flakes have been widely used as conductive fillers for printed stretchable conductors considering their high

[1]School of Materials Science and Engineering, Nanyang Technological University, Singapore 639798, Singapore. [2]School of Electrical Engineering and Automation, Wuhan University, Wuhan, Hubei, 430072, China.
*Corresponding author. Email: pslee@ntu.edu.sg
†These authors contributed equally to this work.
‡Present address: Innovation Center for Textile Science and Technology, Donghua University, Shanghai 201620, China.

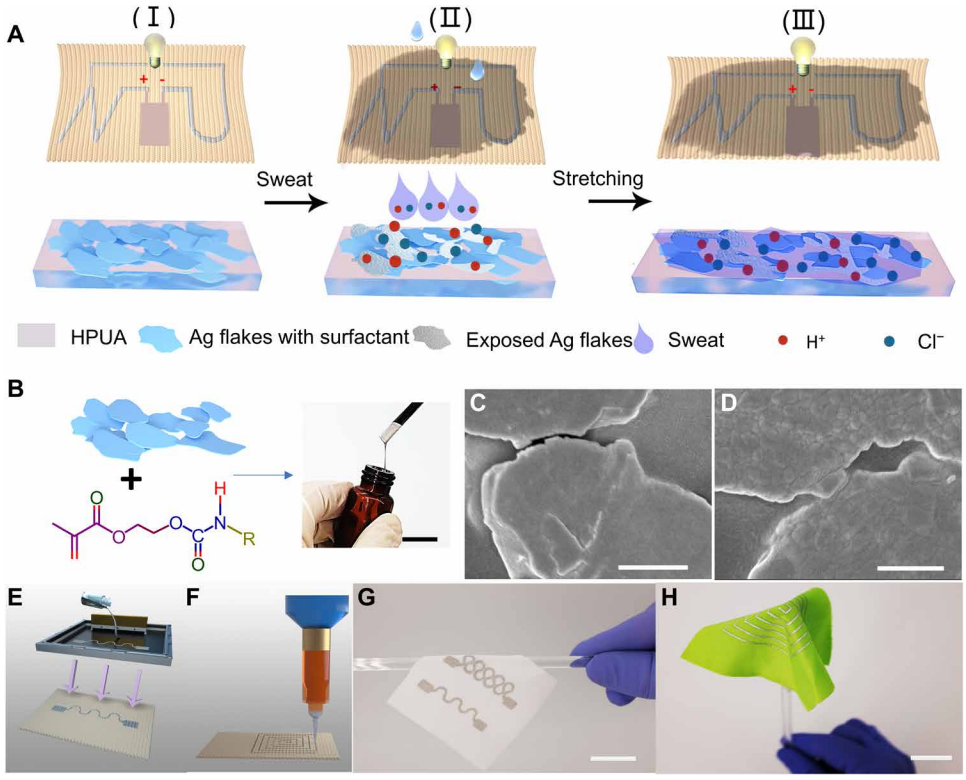

Fig. 1. Schematic of the enhanced conductivity from human sweat and the preparation of the Ag-HPUA electrode. (**A**) Schematic of the enhanced conductivity from human sweat and the surface changes of the printed Ag-HPUA electrodes upon contact with sweat before and after stretching. (**B**) Composition and photo image of the Ag-HPUA ink. Scale bar, 2 cm. (**C** and **D**) SEM images of Ag-HPUA electrode before and after soaking with sweat, respectively. Scale bars, 1 μm. Illustrations of fabrication Ag-HPUA electrodes on the textile by screen printing (**E**) and direct writing (**F**), respectively. (**G** and **H**) Screen-printed and direct-writing patterns on the textile, respectively. Scale bars, 2 cm. Photo credit: Jian Lv, Nanyang Technological University.

conductivity, ease of forming conductive percolation, and scalable manufacturing process (*24*). The massive production of Ag flakes involves the syntheses of Ag nano-/microparticles and subsequent ball milling. To avoid the cold welding and severe oxidation of Ag particles, fatty acid surfactants were added to form a layer of lubricant. The lubricant layer increases the dispersion of Ag flakes in ink formulation but decreases the conductivity of Ag flakes–based electrodes for its electrical insulating nature (*25*). Human sweat is relatively acidic (pH 4 to 6.8) (*26*) and rich in Cl^- ions, and both factors are favorable for the chemical sintering of Ag flakes (*27*, *28*). When the printed electrodes encounter human sweat, the acidic environment and Cl^- work together to partially remove the insulating lubricant layer and increase the contact among adjacent Ag flakes by redepositing Ag from dissolved Ag^+, making the surface of Ag-HPUA electrodes rougher, as shown in Fig. 1 (C and D). This effect enables the printed Ag-HPUA electrode with enhanced conductivity in both original and stretched states compared with dry electrodes without involving sweat (Fig. 1A).

HPUA with ambient photocurable property, hydrophilic nature, and high stretchability was synthesized to serve as the binder to increase the favorability of printing, accessibility of sweat, and endurability to mechanical deformation, respectively. The photo-induced HPUA elastic binder composed of hard segments made up of carbamate groups (-NH-C═O-O-) and soft-segments made up of aliphatic polyether (-O-) or polyester (-CO-O-) backbone is capped with acrylate (C═C) functionality at each end. In the HPUA synthesis, 2-hydroxyethyl methacrylate (HEMA) and polyoxyethylene (POE) are the key components in the design of photocurable HPUA. Beyond acting as the reactive diluent to tune the viscosity of the prepolymer for the ease of printing, HEMA is crucial for the double bond of the acrylate group on the covalent networks (*29*). The POE can enhance the hydrophilicity due to their ether oxygen bonds on soft segments (*30*). The fast ambient photocurable nature of HPUA polymer enables green printing without the massive use of organic solvents and the potential for complex and high-precision structures design in three-dimensional (3D) printing (*31*). Considering the low sweat generation on some occasions, the hydrophilic HPUA binder favors the contact between human sweat and Ag-HPUA electrodes.

Comparing with commonly used thin polymer film substrates, the hydrophilic textile substrate used here facilitates the in situ sweat sampling and as a reservoir. Sweat-reserving capability and porous structure of textiles give prolonged reaction time and enhanced surface area for printed electrodes to contact with sweat. Besides, the component of human sweat varies with gender, secretion area, surrounding, time of day, age, and sweating rate, which will impede the completeness of sintering effects. The textile substrate can be used to prestore active substances, such as lactic acid and Cl^- salt to weaken the effects of irregular sweating behavior of wearers. In our design, the whole electrode fabrication involves the direct printing on textiles, including screen printing and direct writing (Fig. 1, E to H), and then curing in ambient condition without any heat or specific

ultraviolet (UV) curing after possess, which is favorable for both wearable electronics and textile technologies. The elaborate conductive filler selection, well-designed HPUA binder structure, and sweat-soaking friendly textile substrate endowed our printed electrode to be in good contact and reaction with sweat to enhance the conductivity in both relaxed and stretched states.

Synthesis and characterization of HPUA

The photocurable HPUA elastomeric binder was synthesized by a one-pot step-growth polycondensation, followed by radical polymerization from simply available polytetrahydrofuran glycol (PTHF) as a diol, isophorone diisocyanate (IPDI) as a diisocyanate, hydrophilic POE as a chain extender, trimethylolpropane (TMP) as an internal cross-linker, and hydrophilic HEMA as a reactive diluent in the presence of catalyst dibutyltin dilaurate (DBTDL) (figs. S1 and S2). The amount of HEMA was varied at 10, 20, and 30 weight % (wt %) to form HPUA-1, HPUA-2, and HPUA-3. The chemical structure of the multifunctional hydrophilic HPUA elastomer is depicted in Fig. 2A. Prepolymerized intermediates OCN-PTHF-NCO were synthesized by terminating the PTHF diol with an NCO group of IPDI, as shown in fig. S1. Then, OCN-PTHF-NCO was subsequently reacted with hydrophilic POE and TMP to extend the polymer chains and obtain the OCN-PU-NCO prepolymer precursor (fig. S2). The well-designed free radical acrylate (C═C) polymerization mechanism under the UV irradiation ensures the photocurability of HPUA, as shown in fig. S3. PTHF (-OH) was used as the soft segment because its chain is flexible and can facilitate the chain motion for better stretchability (*32*). Among various hard-segment candidates, IPDI (N═C═O) was selected because of its nature of two different reactivity of -NCO groups and stable mechanical performance with nondiscoloring properties (*33*). Furthermore, the IPDI bulky asymmetric alicyclic structure inhibits the crystallization and provides sufficient chain mobility to influence UV curability of HEMA while retaining remarkable tensile properties (*34*). In terms of high hydrophilicity, the secondary -NCO is more active in the presence of DBTDL because of the steric effect, and thus, most of the -OH groups will react with the

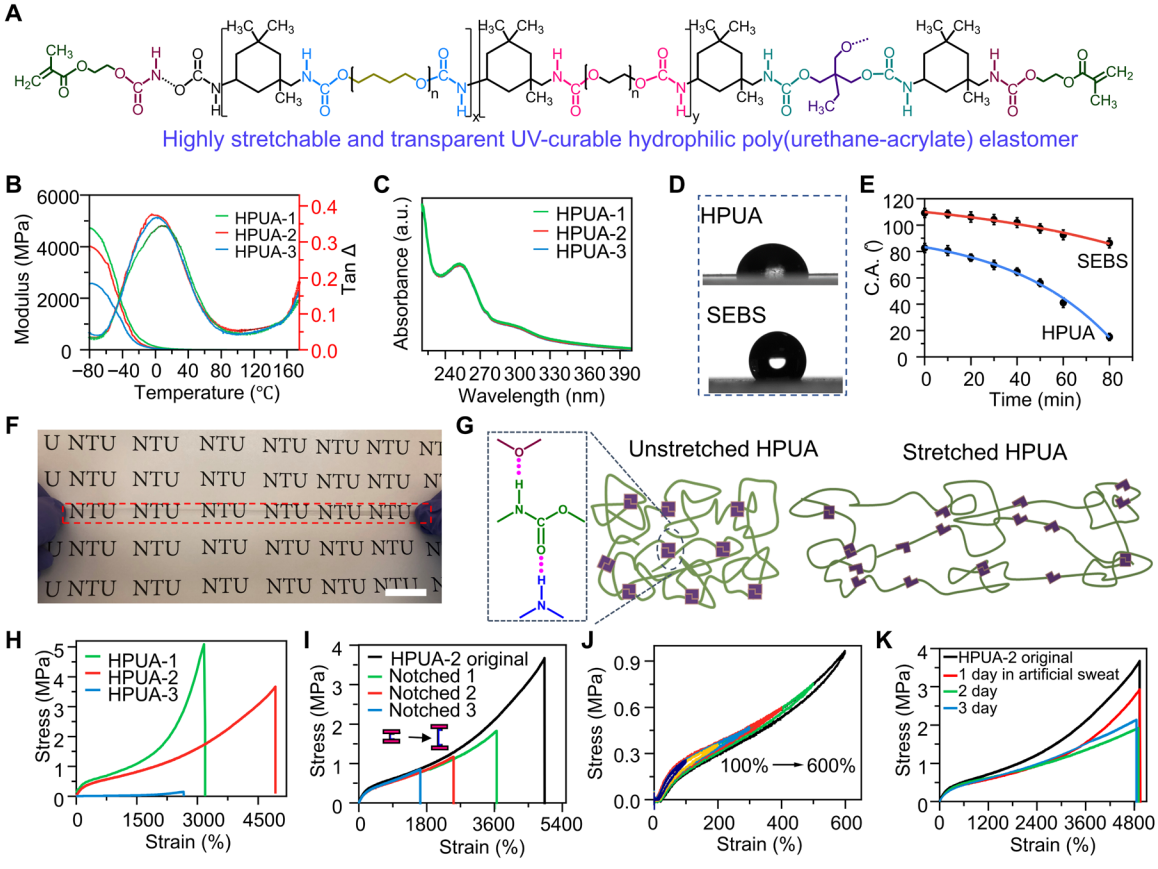

Fig. 2. Hydrophilic HPUA elastomer design and characterization. (**A**) Chemical structure of multifunctional hydrophilic HPUA elastomer. (**B**) Temperature dependence of storage modulus (E) and dissipation factor (tan δ) of HPUA-1, HPUA-2, and HPUA-3 measured by dynamic mechanical analysis under a N_2 atmosphere, at a heating rate of 3°C/min and a frequency of 1 Hz. (**C**) UV-vis spectra of HPUAs with different weight % of HEMA. a.u., arbitrary units. (**D** and **E**) Compared images and the dynamic contact angles (C.A.) of artificial sweat droplet on the HPUA and SEBS glass substrate, respectively. (**F**) Digital photograph of the highly stretchable HPUA film. Scale bar, 3 cm. (**G**) Schematic representation of the reversible covalent bond constructed hybrid dynamic HPUA networks. (**H**) Tensile stress-strain curve of HPUA elastomer films prepared with different molar ratios of HEMA with a sample a strain rate of 100 mm/min. (**I**) Tensile stress-strain curves of the unnotched and notched films of HPUA. A notch of 2.5 mm in length, 1 mm in thickness, a distance of 10 mm, and 5 mm in width. Deformation rate of 100 mm/min. (**J**) Tensile loading-unloading curves of hydrophilic HPUA at different strains of 100 to 600%. (**K**) Tensile stress-strain curves of original HPUA and HPUA soaked in artificial sweat for 1 to 3 days at ambient condition. Photo credit: Jian Lv, Nanyang Technological University.

secondary -NCO, which is helpful to increase the hydrophilicity of the urethane elastomer. POE is selected as the soft segment, because of its hydrophilic cross-linked networks (*35*).

The successful synthesis of HPUA and its intermediates were verified by ^{1}H (proton) and ^{13}C nuclear magnetic resonance (NMR) and Fourier transform infrared spectroscopy (FTIR), and the details are shown in fig. S5 to S7. The FTIR characteristic peaks at 3318 cm^{-1} (N—H) and 1713 cm^{-1} (C═O) stretching vibrations, indicating the formation of -NH-C═O-O groups (fig. S8, A and B). From the FTIR spectra, the disappearance of the characteristic absorption band at 2270 cm^{-1} (-NCO) indicated the completion of the reaction. There are negligible peaks at 1712 cm^{-1} (C═O) and 1635 cm^{-1} (-CH═CH_2), which reveals that the monomer of IPDI has completely reacted with HEMA to make a covalent bond, and the HPUA forms a cross-linked network (fig. S7A). The decrease in the intensity of specific peak at 1635 and 810 cm^{-1} related to -CH═CH_2 bond with increasing ambient UV curing time indicates that the HPUA was fully cured. The thermal properties of HPUAs were characterized by dynamic mechanical analysis (DMA) in tensile mode (Fig. 2B). The glass transition temperatures (T_g) observed from loss factor (tan δ) value of HPUA-1, HPUA-2, and HPUA-3 were 8.52, −4.96, and 3.21, respectively, indicating that the sufficient chain mobility for the reformation of the covalent urethane bonds (NH-C═O-O-). The storage modulus (*E*) reaches a rubbery plateau after T_g and then after continuously drops to nearly zero at high temperature. The thermogravimetric analysis (TGA) shows that the HPUA films exhibit relatively good thermal stability, with displayed two-step weight-loss regions with peak maxima at 280°C and 350° to 450°C, respectively (fig. S9). The UV-visible (UV-vis) absorbance spectra of HPUA-1, HPUA-2, and HPUA-3 are shown in Fig. 2C, and the cutoff wavelengths of the films are in the range of 210 to 400 nm. There two peaks at 240 to 260 nm and 297 to 300 nm are assigned to the urethane carbonyl (C═O) and carbon-carbon double bond of the acrylate groups, respectively, indicating that the HPUA can be photopolymerized under UV illumination. They can produce π*-π* transitions of conjugate carbon-carbon double bond (C═C) and urethane carbonyl (C═O) as shown in the literature (*36*).

Compared with polystyrene-block-poly(ethylene butylene)-block-polystyrene [styrene-ethylene-butylene-styrene (SEBS)], one of the representatives of widely used polystyrene-based block copolymers binder in printed stretchable conductors (*37*, *38*), the synthesized HPUA shows the hydrophilic property to artificial sweat. The contact angle of the HPUA binder is 82.59° and gradually decreases to 15.12° over a period from 0 to 80 min (Fig. 2, D and E, and fig. S10). Such behaviors result in the HPUA having a higher tendency to interact with artificial sweat, owing to their hydrophilic -NH-C═O-O- functionality of the HPUAs (fig. S10). The highly stretchable HPUA films (0.6 mm in thickness) had good optical properties and showed high transparency with a transmittance of ~85% in the visible range of 425 to 800 mm (Fig. 2F and fig. S11). Under the strain, the urethane-based covalent cross-links fix the HPUA networks. Dynamic cross-link based on urethane (-NH-C═O-O-) hydrogen bonds act as sacrificial bonds that can rupture upon loading to dissipate energy and reform after unloading to restore the mechanical properties (schematically illustrated in Fig. 2G).

The tensile-test results showed that the HPUA-2 exhibits superior mechanical properties (Fig. 2H). The high stretchability can be attributed to the presence of a large number of hydrogen bonding in the N-H and C═O urethane regions as shown in fig. S4. The tensile strength and elongation at the break of HPUA-2 were 3.69 MPa and 4954.83%, respectively. The incorporation of HEMA markedly changes the mechanical properties with improved tensile strength and stretchability (fig. S12, A and B). However, the increase of the HEMA content to 30 wt % markedly reduces the stretchability and tensile strength of HPUA-3 owing to the distribution of the hard segments in the carbamate linkage and the reduction in the cross-linking density. The notched HPUA specimen (ASTM D412) exhibited good tear resistance behavior (Fig. 2I and fig. S13, A to D), of which HPUA-2 was the best one. Even with a 2.5-mm notch of the total width (5 mm), it could still bear the strain at breakup to 1569.20% because of its fixing capability on the dynamic cross-links based on hydrogen bonds in the -NH-C═O-O- network structure. Repeated cyclic tensile test and qualitative loading-unloading test were performed, and it showed minimal hysteresis with optimal elastic properties of the HPUA binders because of the strong reformation capability of hydrogen bonds on the N-H group (Fig. 2J). As the electrode needs to be in contact with human sweat, the stability of the HPUA binder in sweat was evaluated by tensile-strain test and FTIR. After soaking in artificial sweat, no change in color could be identified, and the tensile strains of the soaked HPUA-2 film remain the same as the original unsoaked one, confirming the excellent stability in artificial sweat (Fig. 2K). FTIR curves of original HPUA-2 and HPUA-2 after 1 to 3 days of soaking, represent no changes in the molecular structure after long-time artificial sweat absorption (fig. S14). The results presented in fig. S15 show that the weight-swelling ratio of HPUA increases with time and then reaches equilibrium at around 4.5%, suggesting that there is no significant swelling of the HPUA film in the artificial sweat.

Enhanced conductivity from sweat

The viscosity curves of the pure HPUA polymer and the Ag-HPUA ink as the function of shear rate are shown in fig. S16A. Typical shear-thinning behavior appears in both HPUA and Ag-HPUA inks, and the adding of Ag flakes increases the viscosity of HPUA in the range of reported inks for direct writing and screen printing (*39*, *40*). The variation of storage shear modulus (G′) and loss shear modulus (G′′) in HPUA-Ag with the shear stress is shown in fig. S16B in which the G′ is larger than G′′, suggesting that they behave more like solid substance when dropping on the substrate (*39*). The printed electrodes attach well on the top of the textile substrate after printing, as shown in the cross-sectional scanning electron microscopy (SEM) images of the printed Ag-HPUA electrodes before and after soaking with sweat in fig. S17. Uniaxial single and 50% cycling stress-strain curves of the bare and the printed textiles were measured (fig. S18), indicating that printing with a layer of Ag-HPUA electrode has a minor effect on the mechanical properties and recoverability of the textile. Compared with using thin polymer film as the substrate, direct printing of ink on the porous textile makes the bottom part of the electrode fill with fiber bundles and with a higher surface area. This design is favorable for the reaction between the printed electrode and sweat. The hydrophilic fiber bundles introduce the sweat solution to the neighboring area of electrodes, and thus, more reactions among the ions in sweat and electrodes will be initiated, as shown in Fig. 3A and fig. S19.

Meanwhile, the well-designed hydrophilic HPUA binder can enhance the affinity between sweat and the electrode, which is valuable when insufficient sweat is secreted by wearers, especially considering that the pH of sweat generated in the initial sweating period

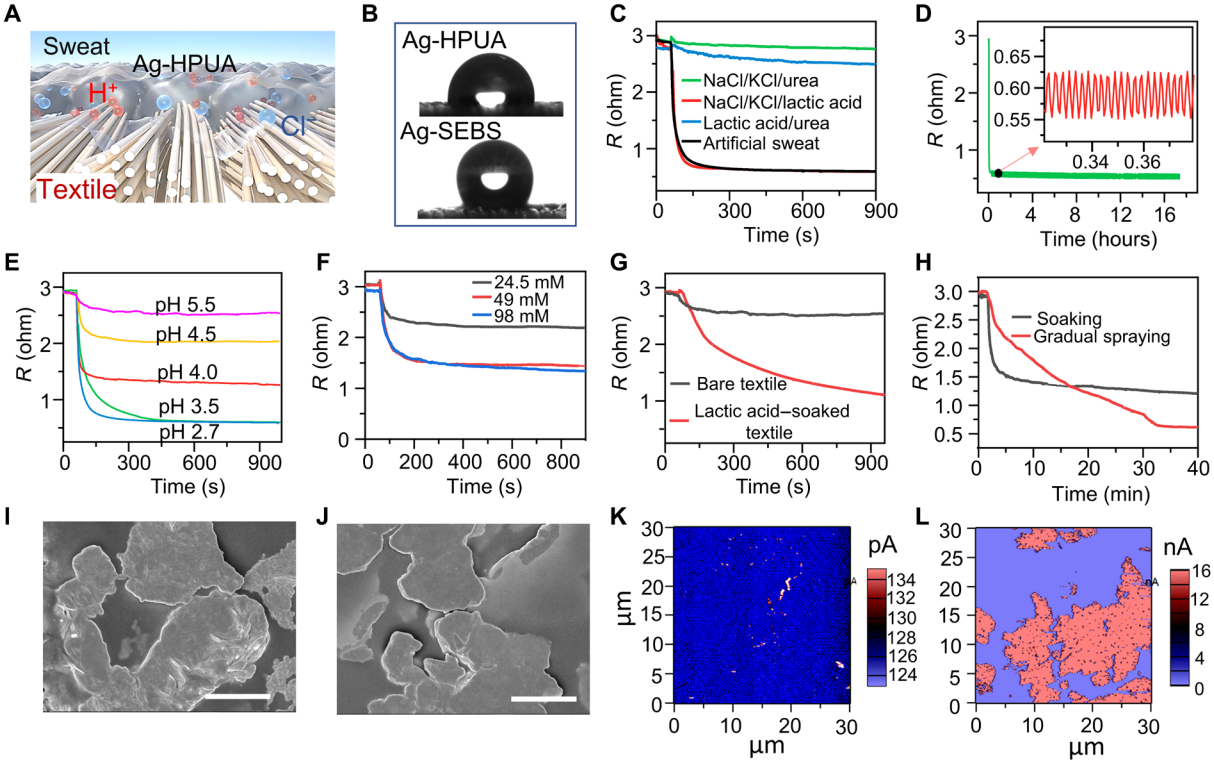

Fig. 3. Characterization and mechanism of the sweat-enhanced conductivity in Ag-HPUA electrodes. (**A**) Scheme of the interface between the textile and the Ag-HPUA electrode as well as the textile-enhanced contact area among active ions and Ag-HPUA electrodes. (**B**) Artificial sweat contact angles of the Ag-HPUA and the Ag-SEBS electrode. (**C**) Resistance changes of Ag-HPUA electrodes after soaking with NaCl/KCl/urea, NaCl/KCl/lactic acid, lactic acid, and artificial sweat solutions, respectively. (**D**) Resistance of an Ag-HPUA electrode on textiles after soaking with the original artificial sweat and subsequent washing by deionized water. The inset is the magnification of the marked area. (**E**) Resistance changes of Ag-HPUA electrodes after soaking with artificial sweats with different pH. (**F**) Resistance changes of Ag-HPUA electrodes after soaking with sweat solutions (pH 4) with different concentrations of Cl^-. (**G**) Resistance changes of Ag-HPUA electrodes printed on the bare (black plot) and 0.4% lactic acid–soaked (red plot) textiles after contacting artificial sweat (pH 5.5). (**H**) Comparison for resistance changes of Ag-HPUA electrodes after applying the sweat (pH 4) by spraying with 2-min intervals and soaking. (**I** and **J**) High-magnification SEM images of Ag-HPUA before and after contact with artificial sweat for 30 min, respectively. Scale bars, 3 μm. (**K** and **L**) Conductive atomic force microscopy of the Ag-HPUA electrode before and after reaction with artificial sweat, respectively.

with a limited amount is relatively lower than that of subsequent sweat and that the lower pH is more preferable for the sintering reaction (*41*). The comparison between the Ag-HPUA and Ag-SEBS electrodes when insufficient sweat (pH 4) is applied on the electrodes is shown in fig. S20. The sweat was sprayed every 2 min, and excessive sweat was sprayed after 30 min. When applied sweat is not enough to cover the surface of electrodes, the Ag-HPUA electrode exhibited a higher resistance drop than that of the Ag-SEBS electrode. This probably comes from the higher affinity between sweat droplets and the Ag-HPUA induced by the hydrophilic nature of the HPUA. The contact angle between the Ag-HPUA electrode and sweat is smaller at around 98.9°, whereas the contact angle between Ag-SEBS electrodes and sweat solution is 128.2°, as shown in Fig. 3B. Both contact angles are higher than respective bare polymer films, resulting from the addition of Ag flakes.

The composition of the original artificial sweat follows the European Standard that contains 87 mM NaCl, 13 mM KCl, 17 mM lactic acid, and 16 mM urea, and the original pH is 2.7 (*42*). The resistance change of the Ag-HPUA electrodes after soaking with four solutions including lactic acid/urea, NaCl/KCl/urea, lactic acid/NaCl/KCl, and original artificial sweat was studied, as shown in Fig. 3C. The original artificial sweat can instantly decrease the resistance of Ag-HPUA electrodes. When enough original artificial sweat without pH tuning was added on Ag-HPUA textile electrodes, the resistance was decreased from 3 to 0.6 ohm in 14 min. The 50 and 90% resistance reduction can be reached after 8.5 and 66 s, respectively, showing the fast reaction between original artificial sweat and printed Ag electrodes. The lactic acid/NaCl/KCl solution has a similar capability with that of artificial sweat to reduce the resistance of electrodes, whereas lactic acid/urea and NaCl/KCl/urea have minor effects within 14 min, suggesting that the enhanced conductivity comes from the synergistic function from lactic acid and NaCl/KCl. The effect of lactic acid and NaCl/KCl was further illustrated in fig. S21. It is clear that even adding a little amount of NaCl/KCl (24.5 mM) and lactic acid (2.125 mM) in lactic acid/urea and NaCl/KCl/urea solution, respectively, the resistance reductions are much more prominent, further confirming that the lactic acid and NaCl/KCl work together to enhance the conductivity of printed electrodes.

To verify the stability of the produced electron-transfer traces, the electrode was immersed in pure water washing with magnetic stirring after the reaction with artificial sweat. The resistance keeps stable at around 0.60 ohm with minor fluctuations (Fig. 3D). This means that the resistance change is irreversible and stable once the

resistance of Ag-HPUA electrodes was reduced by sweats containing both a low pH and a high concentration of Cl^- ions; this conductivity enhancement can be maintained even when the component of sweat fluctuations.

The resistance loss induced by sweats with different pH is shown in Fig. 3E, and the statistical plot of resistance drop and pH with the error bar (n = 3) is shown in fig. S22. The capability of sweat to reduce the resistance of printed Ag-HPUA electrodes increases with the decreasing of pH. As the pH increased from 3.5 to 5.5, the intensity of resistance reduction is gradually decreasing but still obvious within 2 min (Fig. 3D). This pH range covers the pH of most people when no sweat stimulation drugs are used to secrete perspiration, for example, the pilocarpine (*43*). Beyond low pH, the high concentration of Cl^- is also beneficiary for the sintering performance, the effect of Cl^- (pH 4) on the sintering performance was studied in Fig. 3F, and the plot of resistance drop and Cl^- concentration with error bar (n = 3) is shown in fig. S23. The Cl^- concentration in the typical sweat is in the range of 10 to 100 mM (*15*). When the concentration of Cl^- in sweat is 24.5 mM, the resistance of the Ag-HPUA electrode experienced a 26.3% (SD = 3.0%) drop. When increased to 49 mM, the resistance drop is 51.6% (SD = 5.1%), which is close to that of 98 mM (53.7%, SD = 3.1%).

Low pH and high concentration of Cl^- are favorable factors for the sintering reaction between sweat and the Ag-HPUA electrode. In the real application scenarios, the component of human sweat changes with the sweat rate, for example, the pH at high sweating rates is higher than that at low sweating rates (*41*). Reserving enough active species (lactic acid and Cl^-) inside the porous textile substrate can be a way to attain a stable sintering reaction despite acidic and/or Cl^- deficient sweats. We soaked the textile in a 0.4% lactate solution and then dried it to store lactic acid in the textile before printing the electrodes on. When the textile contacts with water, the reserved lactic acid will dissolve immediately and take part in the sintering reaction. As shown in Fig. 3G, the lactic acid–soaked textile electrode shows a much significant resistance drop than the electrode printed on the bare textile after soaking in pH 5.5 artificial sweat. The slower reaction than that from low-pH artificial sweat–soaked samples is probably related to the dilution process of the concentrated lactic acid.

In addition, in the real sweating behavior, the insufficient secreted sweat at the initial period typically appears in the form of droplets. We applied the artificial sweat (pH 4) on the Ag-HPUA by spraying after every 2-min interval to mimic the real sweating behavior. As shown in Fig. 3H, as the sweat was gradually sprayed on the Ag-HPUA, the resistance did not experience a steep drop as insufficient sweat was applied. The final resistance of Ag-HUPA sprayed by sweat is around 0.62 ohm, which is much lower than that (1.21 ohms) of the electrode treated by immersing in the same sweat. This means that the real sweating behavior is favorable in attaining the low resistance from the sweat-induced sintering reaction. The significant difference may come from the involvement of more O_2 at the air-sweat-electrode ternary interfaces and the accumulation of active species induced by the faster evaporation of sweat droplets.

The fast resistance drop likely comes from the reaction between the exposed Ag flakes of the Ag-HPUA electrode and sweat instead of the interaction/reaction between the inner Ag flakes. The change in resistance is faster than the drop in contact angle as a function of time (fig. S24), indicating that the surface Ag flakes reacting with the sweat play dominant roles in the resistance reduction. The SEM images of electrodes before and after the reaction with artificial sweat are shown in fig. S25 and Fig. 3, I and J. Original artificial sweat with pH 2.7 was chosen to clearly show the reaction between artificial sweat and printed electrodes. The Ag-HPUA matrix keeps intact after reacting with artificial sweat. However, the surface of exposed Ag flakes becomes coarser, and some adjacent flakes merge as shown in high-magnification SEM images.

To further unveil the reaction between the Ag-HPUA and artificial sweat, Ag flake powders were immersed inside the urea, lactic acid/urea, NaCl/KCl/urea solutions, and artificial sweat. The lubricant layer on the surface of Ag flakes is made from hydrophobic fatty acid. This is the reason why most Ag flakes in urea solution, lactic acid/urea, and NaCl/KCl/urea solution stay on the top of solutions, as shown in fig. S26. However, all silver flakes aggregated together and dropped to the bottom of the glass vials in the artificial sweat solution, suggesting that artificial sweat containing both lactic acid and Cl^- ions causes the most intensive reaction with Ag flakes. The SEM images of Ag flakes after mixing with different solutions are shown in fig. S27. Similar to the exposed Ag flakes in Ag-HPUA electrodes, the surface of artificial sweat-treated and NaCl/KCl/urea-treated silver flakes become coarser, whereas lactic acid/urea-treated Ag flakes have a smooth surface as that of pristine silver flakes, showing that the Cl^- is the key factor to induce the surface roughness change. Although there is slight aggregation in the NaCl/KCl/urea solution and a coarse surface on Ag flakes is resulted, solely having Cl^- ions cannot fully remove the surfactants on the flakes (as evident from the partial settling of Ag flakes at the bottom of the glass vial). The coexistence of lactic acid and NaCl/KCl would be essential for the sweat sintering of Ag flakes.

It has been reported that both H^+ and Cl^- can remove the lubricant and increase the conductivity of the Ag-based electrodes (*27*, *28*, *44*). The long-term resistance change of Ag-HPUA electrodes after soaking lactic acid/urea and NaCl/KCl/urea is shown in fig. S28. In the presence of lactic/acid/urea and NaCl/KCl/urea solutions, the resistances of the Ag-HPUA electrodes experienced a continuous reduction in 15 hours, coming from the effects of H^+ and Cl^-, respectively, although both of them have minor declination within 14 min. Especially, after 6 hours, the Ag-HPUA electrodes with NaCl/KCl/urea and lactic acid/urea solutions start to go through faster resistance reduction that may result from the evaporation-induced high concentration of Cl^- ions and lactic acid.

Lactic acid plays a similar role as the short-chain acids—such as malonic acid, adipic acid (*45*), acetic acid (*46*), and sulfuric acid (*47*)—which could partially or fully remove or reduce the fatty acid–based lubricants. Besides, H^+ is helpful in the dissolution of Ag with the presence of O_2 through the following reaction (*48*, *49*)

$$4Ag + O_2 = 2\,Ag_2O \quad (1)$$

$$Ag_2O + 2\,H^+ = 2\,Ag^+ + H_2O \quad (2)$$

However, the reaction between Ag-HPUA and urea/lactic acid solution is not obvious because the concentration of lactic acid is low at 0.1% and lactic acid is a weak acid that is hard to dissociate completely to release H^+ for lubricant removal and the release of Ag^+. Beyond removing the lubricant, the Cl^- ions have adverse effects on the dissolution and agglomeration of Ag flakes. On one hand, the Cl^- ions have a high affinity with Ag^+, which will accelerate the dissolution of Ag^0 to Ag^+. The Cl/Ag ratio decides the interaction

between Ag and Cl^- to form insoluble AgCl or soluble $AgCl_x^{1-x}$ species (*50*). The low Cl/Ag ratio forms AgCl that impedes the further dissolution of Ag^0, whereas the high ratio induces the formation of soluble Ag-Cl species that increases the dissolution rate (*51*). In our case, the ratio of Cl/Ag is relatively high, and a negligible amount of insoluble AgCl was formed because of the lubricant layer that limited the exposed surface area of Ag flakes. The x-ray diffraction (XRD) in fig. S29 shows that all the diffraction peaks of NaCl/KCl/urea and artificial sweat–treated Ag flakes belong to Ag, and no AgCl and other impurities are detected. The x-ray photoelectron spectroscopy (XPS) survey scans in fig. S30A show that weak Cl 2p peaks can be detected in NaCl/KCl/urea and artificial sweat–treated Ag flakes. The peaks at 199.6 and 198 eV can be assigned to Cl $2p_{1/2}$ and Cl $2p_{3/2}$ of AgCl, respectively, as shown in fig. S30B (*52*). Both Ag^0 and Ag^+ with the spin-orbit doublets (the separation is 6 eV) can be found in Ag 3D spectra (fig. S30C). The atomic percentage of Ag^0 in Ag flakes is 83%. After treatments with NaCl/KCl/urea and artificial sweat, the fraction of Ag^0 increased to 90 and 94%, respectively, suggesting that most of the newly formed nanoparticles are Ag.

In the dynamic equilibration of Ag^0-Ag^+ system, some Ag^+ can redeposit to Ag^0. The Cl^- ions induce the aggregation of Ag^0 by decreasing the surface double electrical layer of the Ag particles via elongated ionic length and partially destroying the absorbed lubricant surfactant at high concentration (*28*, *53*). As a result, the redeposited Ag (mostly) and precipitated AgCl make the Cl^--treated Ag flakes coarser and more liable to aggregation compared with lactic acid/urea-treated Ag flakes. However, most of the NaCl/KCl/urea-treated Ag flakes still float on top of the solution, and Ag-HPUA electrodes experience a minor resistance drop within 14 min, probably due to the limited capability of low-concentration Cl^- ions to remove the lubricant and sinter the Ag flakes.

Synergistically, the combination of low-concentration lactic acid and Cl^- ions induces the enhanced aggregation of silver flakes and fast resistance drop of Ag-HPUA electrodes because of the augmented capability to remove lubricant surfactant and accelerate dissolution/redeposition of Ag. TGA was applied to detect the weight % of lubricant in Ag flakes. The result in fig. S31 clearly shows that the remaining weight of artificial sweat–treated Ag flakes is 99.8%, which is higher than that of pristine, lactic acid/urea, and NaCl/KCl-treated Ag flakes, suggesting that the artificial sweat containing lactic acid and Cl^- ions is the most powerful solution to remove the lubricant. Also, the atomic ratio of C/Ag in the XPS spectrum decreased from 1.96 to 0.62 (fig. S30D). However, lubricant cannot be fully removed by artificial sweat. The FTIR result of Ag flakes treated with artificial sweat in fig. S32 shows that the functional groups from the lubricant layer remain on the surface of Ag flakes after the reaction with artificial sweat. The deprotonated carboxylate bands at 1635 and 1577 cm^{-1} are observed, which are attributed to $\nu(COO\text{-})_{asym}$ and $\nu(COO\text{-})_{sym}$, respectively (*54*), resulting from the lubricant layer on the surface of Ag flakes. The removal of lubricant weakens the physical barrier and favors the reaction among Ag flakes, lactic acid, and Cl^- ions.

During the reaction between artificial sweat and Ag-HPUA electrodes, certainly, some Ag^+ ions redeposit on the exposed Ag flakes, although the dissolution of Ag is also taking place. In the junction area, the surface potential is higher than other surface areas; the dissolved Ag^+ ions may be more prone to redeposit in the conjunction area, resulting in the fusion of the adjacent Ag flakes and enhanced electrical conductivity (*44*). The conductive atomic force microscopy (C-AFM) comparison shows that the surface of electrodes turns to be more conductive after reaction with artificial sweat (Fig. 3, K and L, and fig. S33). These surface changes probably result from the reaction between the exposed Ag flakes and artificial sweat and account for the sweat-induced conductivity increment of the printed electrode.

Sweat-enhanced conductivity during stretching

The durability of electrodes to mechanical deformations caused by the wearer's daily activities, especially for stretching, can guarantee wearable devices to work properly under and after the strain. Because of the flowing property and fast curing of the Ag-HPUA ink, the formed electrodes cannot penetrate deeply and fully cover the surface of each fiber; instead, the cavities of the textile substrate are filled and fiber bundles are bonded by printed inks. This behavior is not favorable for stretchable textile electrodes, because the strain from the deformed textile substrates will transmit fully to the printed electrode by the movement of fibers (*20*, *55*). However, the synthesized highly stretchable and elastic HPUA binder can resist the formation of obvious cracks on the Ag-HPUA electrodes upon 50% strain, as shown in Fig. 4A. When the printed electrodes were soaked with artificial sweat and then stretched, both the initial resistance and the resistance increment under stretching are lower than that of the original Ag-HPUA electrode (Fig. 4B). Also, a low pH is favorable for sintering reaction under stretching, and the resistances of pH 4 sweat and original artificial sweat (pH 2.7)–soaked electrodes increased from 0.57 to 82.5 ohms and 0.36 to 3.5 ohms, respectively.

During the stretching with the presence of artificial sweat, the separation of Ag flakes and the sintering reaction take place simultaneously. Stretching makes Ag flakes inside the HPUA matrix slide with each other to accommodate the imparted strain, showing in the form of resistance increase. The reaction between artificial sweat and Ag-HPUA electrodes can create new electron transfer paths during the stretching and counteract stretching-induced conductivity loss. The SEM images of the dry and sweat-soaked electrodes under 50% stretching are shown in Fig. 4C [(I) and (II), respectively], and (III) and (IV) in Fig. 4C are the corresponding higher magnifications. Under the stretching, more Ag flakes inside Ag-HPUA electrodes are exposed and react with human sweat, making the surface of Ag flakes coarser than that of the dry electrode, which agrees well with the observations in nonstretched electrodes.

The sweat-induced sintering reaction also significantly increases the electrode's durability to cyclic tensile deformation which is super catastrophic in real application scenarios, as shown in Fig. 4D. Without sweat, the resistance of the printed electrodes increased to more than 40 kilohm at the strained state and 5 kilohm at the released state. In contrast, the pH 4 sweat enables the electrode to have a much less resistance increment after 100 cycles of 30% stretching, maintaining at 2.4 ohm at the strained state and 0.76 ohm at the relaxed state. The original artificial sweat with pH 2.7 is more powerful to minimize the resistance increment caused by cycling stretching. The effect of sweat in reducing the stretching-induced resistance increase is more distinct in cyclic stretching than in single 120% stretching, resulting from the prolonged reaction-induced continuous generation of electron transfer paths. The resistance at both the stretched state and the relaxed state keeps dropping with the continuous cycling stretching, which is opposite with previously reported printed stretchable Ag flakes–based electrodes (*20*).

In our design, the stretchable HPUA binder can hold the conductive fillers together, and the sintering reaction is responsible for

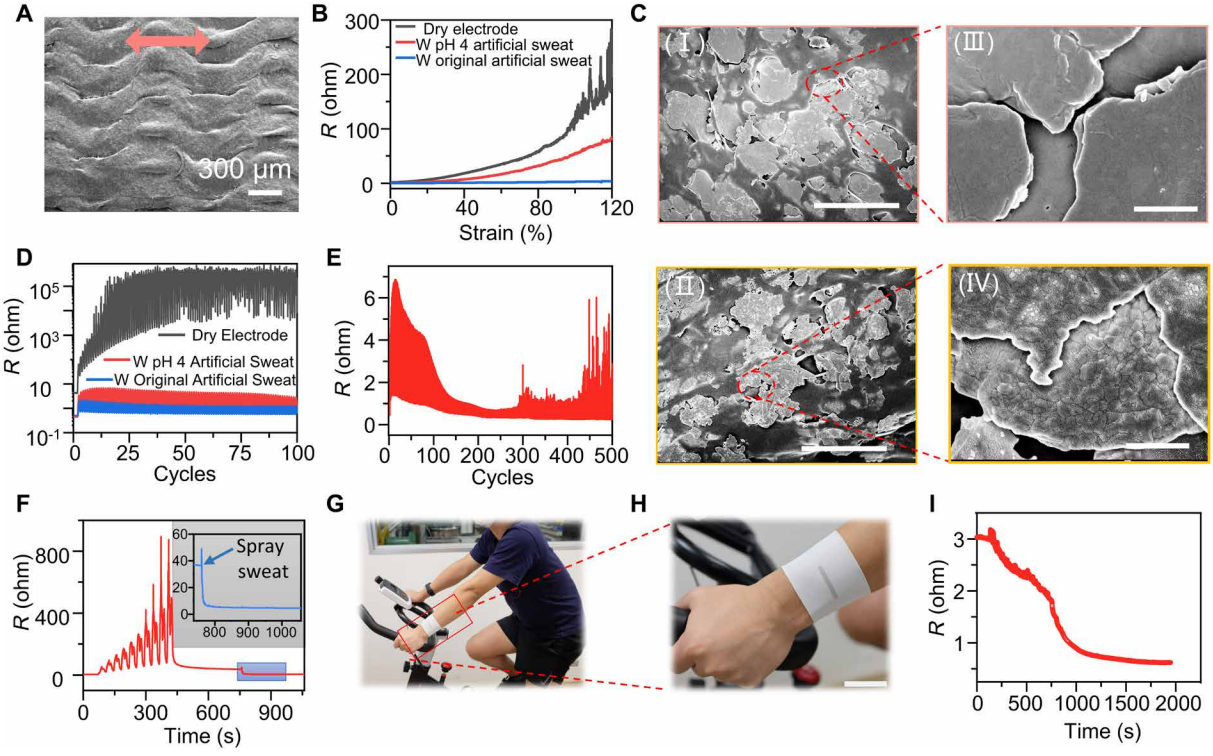

Fig. 4. The effect of sweat on the stretched Ag-HPUA electrode and on-body real-time test. (**A**) SEM image of the artificial sweat-soaked Ag-HPUA electrode on textiles under 50% stretching and the arrow shows the stretching direction. Scale bar, 300 μm. (**B**) Resistance versus strain plots of the Ag-HPUA textile electrode without (black plot) and with the presence of artificial sweat (pH 4) (red plot) and original artificial sweat (blue plot). (**C**) Low-magnification (I and II) and high-magnification (III and IV) SEM images of the stretched Ag-HPUA electrode before and after soaking with original artificial sweat. Scale bars, 20 μm (I and II) and 2 μm (III and IV). (**D**) Resistance changes of the Ag-HPUA textile electrode under 30% cycling stretching without (black plot) and with the presence of artificial sweat (pH 4) (red plot) and original artificial sweat (blue plot). (**E**) Resistance changes of the Ag-HPUA textile electrode during 500 cycles of 30% stretching in the presence of artificial sweat (pH 4). (**F**) Resistance changes of one Ag-HPUA textile electrode experiencing the first 10 cycles of 30% stretching and subsequent artificial sweat (pH 4) spraying . The inset is the magnification of the marked square. (**G** and **H**) Photo images of anchoring the printed Ag-HPUA electrode on one subject's forearm for real-time testing. Scale bar, 3 cm. (**I**) Resistance changes of one Ag-HPUA electrode during the whole stationary cycling exercise of the subject. Photo credit: Jian Lv, Nanyang Technological University.

creating new conductive networks, making sweat (pH 4)–soaked Ag-HPUA electrode maintain low resistance at both released status (0.26 ohm) and stretched status (5 ohm) even after 500 cycles of 30% stretching (Fig. 4E). Even after washing with water and drying, the sweat-treated sample still can maintain lower resistance upon cycling stretching compared with that of the original Ag-HPUA electrode, as shown in fig. S34. When repeating with the same process, the resistance maintains low. The acidic sweat also can repair the conductivity loss of electrodes caused by stretching. As shown in Fig. 4F, the resistance of the dry Ag-HPUA electrode increased from 2.62 to 36.7 ohm after 10 cycles of 30% stretching, and then the spraying of pH 4 artificial sweat could reduce the resistance to less than 5 ohm within 2 min, further showing the ability of sweat in reducing the resistance of stretchable Ag-HPUA electrodes (movie S1).

The real-time study was carried out by monitoring the resistance change of Ag-HPUA electrodes wrapped on the subject's arm when the subject was doing the stationary cycling to initiate the sweating, as shown in Fig. 4 (G to I). The test was conducted under the approved IRB-2017-08-038-02. The initial resistance is around 3.02 ohm and dropped to 0.62 ohm after 27-min cycling, demonstrating the practical capability of sweat to reduce the resistance of Ag-HPUA electrodes. For real application scenarios, the amount of released Ag^+ into the sweat is crucial to evaluate the toxicity of Ag-HPUA electrodes because the Ag^+ is the most detrimental form of Ag element to human skin. As shown in fig. S35, the release of Ag^+ into the sweat is around 1.26 μg/cm^2 area of Ag-HPUA electrodes after 12 hours, which is in a range comparable with commercial Ag nanoparticle-coated antibacterial textiles, although our electrodes contain higher Ag loading (36.5 wt %) than the commercial antibacterial textiles (with <0.02 wt % Ag loading) (*56*). This is because most of the Ag flakes are wrapped by HPUA that would prevent contact among inner flakes and sweat.

Demonstration for wearables

The capability of sweat to enhance the conductivity of Ag-HPUA electrodes provides more guidance into the design of the wearable electronics that need to have intimate contact with human skin as sweat is one of the most liable biofluids secreted by the human body. To demonstrate the application of sweat sintering reaction, we designed the first example of a textile-based stretchable Zn-Ag_2O sweat battery that uses human sweat as the electrolyte and Ag-HPUA electrodes as stretchable current collectors to provide energy for wearable electronics. The structure of the stretchable sweat-activated battery is shown in Fig. 5A. The printed Zn electrode was selected as the anode, and Ag_2O served as the cathode,

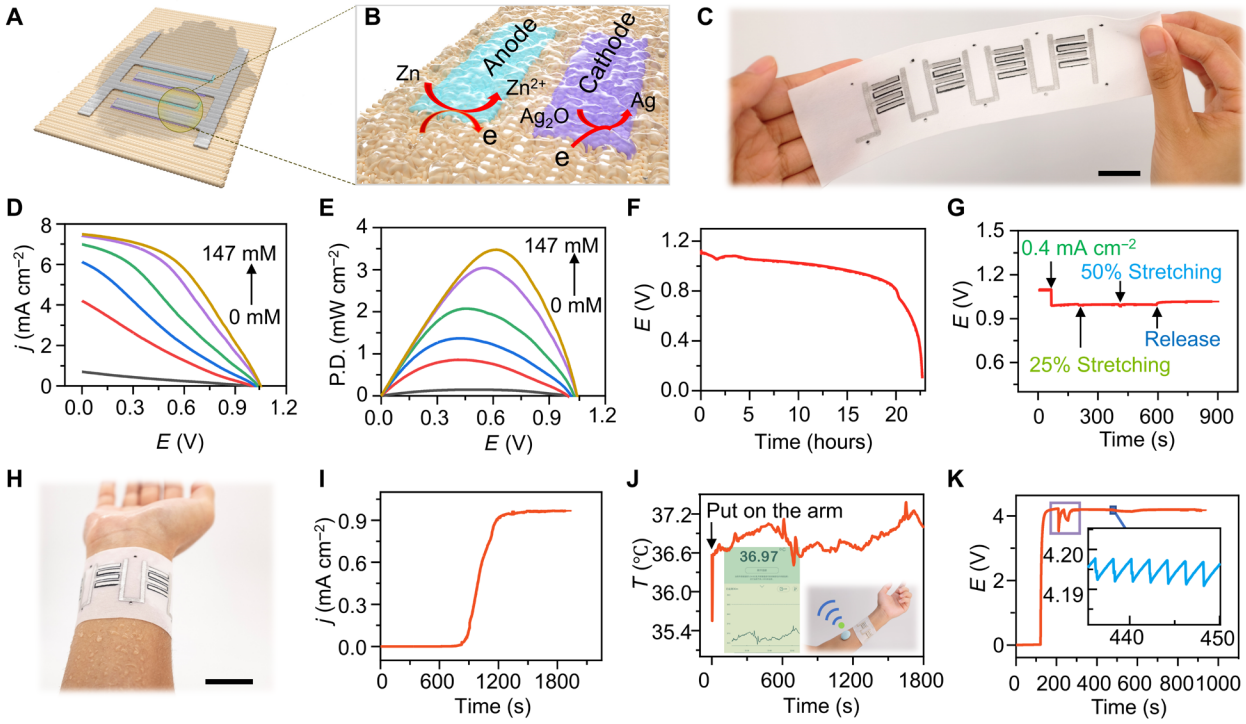

Fig. 5. Demonstration of the stretchable sweat-activated battery using Ag-HPUA electrode as the current collector. (**A**) and (**B**) Scheme and reaction mechanism of the printed sweat-activated Zn-Ag_2O battery on the textile. (**C**) Photo image of four printed Zn-Ag_2O batteries connected in series. Scale bar, 2 cm. (**D**) Polarization curve and (**E**) power density (P.D.) curve plots of the sweat-activated battery in the presence of artificial sweat (pH 4) with different Cl^- concentrations from 0 to 147 mM. (**F**) Long-time discharge curve of the printed Zn-Ag_2O battery at the current density of 0.2 mA/cm^2. The electrolyte used here is the sweat (pH 4) with 87 mM NaCl, 13 mM KCl, 17 mM lactic acid, and 16 mM urea. (**G**) Discharge curves of two printed Zn-Ag_2O batteries using the Ag-HPUA as the conductors under 25 and 50% stretching. (**H**) Photo image of the printed batteries band on the subject's arm. Scale bar, 3 cm. (**I**) Real-time current density versus time plot of printed battery during the stationary cycling exercise of the subject. (**J**) Real-time temperature curve of the wearable temperature sensor powered by four series-connected Zn-Ag_2O sweat batteries. The inset shows the screen of the smartphone and the setup of the temperature sensor and printed batteries when the self-powered sensing system is working. (**K**) Voltage changes of the supercapacitor charged by four Zn-Ag_2O sweat batteries during powering the wearable temperature sensor. The black square is the sensor and smartphone connecting period. Photo credit: Jian Lv, Nanyang Technological University.

respectively. Besides serving as the sweat absorbent and separator, the porous textile substrate also enables the high loading of electrode inks, as shown in Fig. 5B. In the presence of human sweat, electrons are generated on the anode from Zn flakes and then transferred to the cathode through external loading to reduce Ag_2O to Ag. Compared with the reported sweat-activated battery (*19*), the scalable and pattern-designable printing technology facilitates the massive and cheap manufacturing of the sweat-activated batteries, as shown in Fig. 5C.

The linear sweep voltammetry curves and power curves of the stretchable sweat-activated battery using artificial sweat electrolyte with the increased concentration of NaCl were shown in Fig. 5 (D and E), respectively. The power density of the printed batteries is boosted from 0.149 to 3.47 mW/cm^2 when the concentration of NaCl increased from 0 to 147 mM. At a discharging current of 0.2 mA/cm^2 (Fig. 5F), the capacity of the battery is around 4 mAh/cm^2, which is comparable to the reported stretchable Li-ion battery (*57*). With the presence of sweat, the new conductive networks can be formed on Ag-HPUA current collectors by the reaction between Ag flakes and sweat, making the sweat batteries work properly under external strain. As shown in Fig. 5G, 25 and 50% stretching cause a minor change to the voltage of the battery when it was discharged at a current density of 0.4 mA/cm^2.

The durability of mechanical deformation enables the printed batteries to generate energy properly on the subject's forearm during the secretion of sweat (Fig. 5H). The current density of a printed battery with 1-kilohm external loading was increased from 0 to 0.97 mA/cm^2 after 16-min exercise and maintained at this level afterward (Fig. 5I), demonstrating the practical workability of the human sweat to serve as the biocompatible electrolyte for Zn-Ag_2O batteries. As the coronavirus 2019 is plaguing the world, the continuous monitoring of the body temperature is valuable in the prevention of infection (*58*). Printed stretchable sweat batteries can serve as the power source to power a commercial wireless temperature sensor monitoring the temperature on the hand of the subject and sending the data to the smartphone, as shown in movie S2, fig. S36, and Fig. 5J. Ecoflex was printed to confine each battery for avoiding the short circuit. A 5.6-mF capacitor was used to buffer the energy generated by batteries, and the voltage change of the capacitor and the current change of the circuit are shown in Fig. 5K and fig. S37, respectively. After enough sweat was secreted by 16-min exercise, four series-connected batteries can charge the capacitor to 4.17 V in 40 s, and then the sensor started to send high current pulse signals to connect the smartphone and send real-time temperature data. The average power needed in the pairing period and data sending period are less than 0.24 and 0.162 mW, respectively. The batteries

can timely compensate the consumed energy in the capacitor in both the connecting period and data sending period. Especially in the connecting period, the consumed energy by the wireless circuit is higher, and our batteries still can supply enough energy for the sensor to work properly.

DISCUSSION

In summary, we designed printable, photocurable, and textile-based Ag-HPUA electrodes of which the resistance can be reduced by human sweat in both original and stretched states. The electrodes compose of Ag flakes and HPUA binder with hydrophilic, photocurable, and high stretchable properties. Within the elaborately designed HPUA binder, hard segments made up of carbamate groups (-NH-C═O-O-) and soft segments made up of aliphatic polyether (-O-) or polyester (-CO-O-) backbone were capped with acrylate (C═C) functionality at each end. When the Ag-HPUA encounters the sweat, the lactic acid and Cl^- work synergistically to enhance the conductivity rapidly and permanently by removing the lubricant and sintering the exposed Ag flakes. The affecting factors and mechanism of the reaction between the Ag-HPUA electrode and sweat were well explored. The sweat also can significantly improve the electrode's durability to stretching deformation. The on-body test has shown that the resistance of the electrode can be reduced from 3.02 to 0.6 ohm after the subject started to secrete sweat. Further research will explore the effects of other components in sweat and wearing behaviors, such as the heat transferring from the human body, on the sintering reaction. Nevertheless, the enhanced conductivity coming from human sweat demonstrated in our work enriches the design of stretchable wiring electrodes and skin-mountable devices. As an example, a type of stretchable sweat-based Zn-Ag_2O battery using Ag-HPUA as the current collector was directly printed on textile to supply energy for a wearable wireless temperature sensor. Apart from acting as the electrolyte, human sweat also enables the battery to work properly under stretching by sweat sintering of the current collector. Our method uses sweat that is unharmful to human skin as the sintering agent that reduces the resistance of printed stretchable electrodes during wearing, providing a new route in the design of printed stretchable devices.

MATERIALS AND METHODS

Materials

PTHF [M_w (weight-average molecular weight) = 1000 g/mol, 98%] and POE (M_w = 1000 g/mol, 98%) were purchased from Sigma-Aldrich and degassed at 130°C for 3 hours before use. TMP (M_w = 134.17 g/mol, 97%), DBTDL (95%), HEMA (M_w = 130.14 g/mol, ≥99 DBTDL (M_w = 631.56 g/mol, 95%), acetone (anhydrous ≥99.5%), sodium chloride, DL-lactic acid (~90%), potassium chloride, sodium hydroxide, and urea were also received from Sigma-Aldrich and used without any purification. IPDI (a mixture of isomers, 98%), methyl ethyl ketone (MEK; ≥99%), 1-hydroxycyclohexyl phenyl ketone (IRGACURE 184; M_w = 204.3 g/mol, 99%), Ag flakes (10 μm), the SEBS (Tuftec H1052) with 20/80 S/EB weight ratio, and the hydrophilic textile were obtained from Alfa Aesar, Fisher Chemical, Ciba Specialty Chemicals, Puwei Applied Materials Technology, Asahi Kasei Corporation, and MHTC Technology Company, respectively. Deuterated solvents for NMR characterization were obtained from Cambridge Isotope Laboratories Inc. Deionized water was used throughout the study.

Elastomer characterization

^1H NMR spectroscopy (400-MHz Bruker DPX 400), ^{13}C NMR (400-MHz Bruker DPX 400), and FTIR (FTIR-ATR, PerkinElmer, Frontier) were systematically investigated to understand the chemical structure of the synthesized UV-curable hydrophilic HPUA. ^1H (proton) and ^{13}C NMR were carried out at ambient temperature using deuterated solvents as the lock and the residual solvent or tetramethylsilane signal as the internal standard. The thermal property of the HPUA film was characterized using TGA (TA Instruments Q50). HPUA samples (10 to 25 mg) were placed in a platinum pan and heated from room temperature to 700°C under a nitrogen atmosphere at a heating rate of 10°C/min. DMA analysis was conducted on a dynamic mechanical analyzer (DMA; TA Instruments, DMA Q800), and samples were measured in a temperature range of −80° to 170°C using a heating rate of 10°C/min in a liquid N_2 environment. UV-vis absorption and transmission spectra were recorded with a spectrometer (Shimadzu, UV-2501 PC) in the range of 190 to 900 nm at ambient temperature. All tensile test samples were prepared according to ASTM D638-10, and mechanical stress-strain was obtained with Materials Testing Systems (MTS) criterion model 43 (MTS Systems Corporation, Eden Prairie, MN, USA) static mechanical tester with a load cell of 500 kN at a strain rate of 100 mm/min at room temperature. Dynamic contact angles of artificial sweat on the Ag-HPUA surface of the prepared films were measured at ambient temperature using a contact angle meter (Data Physics OCA 15 Pro).

Synthesis of NCO-functionalized urethane prepolymers (OCN-PTHF-NCO)

PTHF (14.50 mmol) was charged in a dried three-necked glass vessel equipped with a thermometer, a mechanical stirrer, a condenser, and an nitrogen atmosphere at 100°C for 1 hour to remove any moisture and then reduced to 85°C. Isophorone diisocyanate (44.95 mmol) and catalyst (DBTDL, 0.2 wt % PTHF and IPDI, 2000 parts per million) dissolved in MEK (5 ml) were added dropwise into the vessel, and the resultant mixture was kept stirring at 85°C for 6 hours under an N_2 atmosphere to yield OCN-PTHF-NCO. Afterward, 20 ml of dry MEK was added to dissolve OCN-PTHF-NCO.

Synthesis of HPUA

A typical procedure of the preparation of the HPUA and their chemical structures are shown in fig. S2. The two-step synthesis routes were described briefly as follows: First, POE (14.50 mmol) and TMP (7.25 mmol) were added to the OCN-PTHF-NCO prepolymer solution. The reaction was carried out at 85°C for another 4 hours with nitrogen protection, and then 20 ml of MEK was added to reduce the viscosity and prevent gelation. The rate of reaction has been monitored by the *n*-butyl amine back titration method according to ASTM D 2572-97. After the synthesis of the OCN-PU-NCO, the reaction mixture cools down to 60°C, and then OCN-PU-NCO was end-capped with the required amount of HEMA. The resulting HPUA mixture was further stirred for 2 hours at 60°C under nitrogen atmosphere to ensure that all isocyanate (-NCO) groups were consumed. FTIR spectra were collected at regular time intervals, measuring the progressive decrease of the isocyanate (-NCO) region at 2270 cm^{-1}. The peak associated with the -NCO group disappears in the final synthesized HPUA, and thus, it signifies the formation of HPUA end-capped with acrylate double bonds.

Fabrication of HPUA film

The freestanding film of HPUA was prepared as follows: The synthesized HPUA was diluted with anhydrous 2-butanone (85 wt %) and stirred at 40°C for 30 min. After a perfect mixing, 1 wt % 1-hydroxycyclohexyl phenyl ketone of the total weight of the HPUA resin was added and stirred for another 30 min at room temperature to obtain a homogeneous HPUA mixture. The resulting HPUA resin was then poured onto a glass petri dish and irradiated by a medium pressure UV lamp (365 nm) for 30 min, with a distance of 8 to 10 cm from the UV lamp to the focal point of the samples. The petri dish was coated with a releasing agent to prevent adhesion of HPUA resin and easily release from the petri dish. The resultant HPUA films were peeled off and placed into the desiccator at the ambient condition for further analysis. The curing behavior of the HPUA film was analyzed by observing the changes in the absorption band of the acrylate group (C═C) at 1634 and 810 cm^{-1}.

Formulation of the ag-HPUA ink and electrode printing

The amber glass vials were used as containers to avoid the photocuring of the ink before printing. HPUA (0.75 g) was mixed with 1 g of Ag flakes by shaking for 10 min. A stainless-steel stencil (Micro Tech Technology, Shenzhen, China) fabricated by laser cutting with a thickness of 200 μm was applied to perform the screen printing. Electrode patterns are designed on AutoCAD software. The electrodes were directly printed on top of the textile in a laboratory-made black box and then cured in the ambient laboratory environment for 30 min. A 3D printer called System 30 M manufactured by Hyrel 3D (USA) with a 0.36-mm nozzle was used to perform the 3D printing on textile. The printing speed is 10 mm/s, and the curing process was finished in a room environment without heating and UV lighting.

Formulation of the ag-SEBS ink

The Ag-SEBS ink was formulated by mixing Ag flakes with SEBS resin (3 g of SEBS/10 ml of toluene) at a weight ratio of 1:0.75 under the shaking.

The characterization of printed Ag-HPUA electrodes

The sweat-enhanced conductivity was performed by using a multimeter (DAQ6510, Keithley) to test the resistance change of electrodes with one-pass printing (length, 2 cm; width, 0.3 cm) after adding the artificial sweat. The artificial sweat was prepared on the basis of European Standard, and pH was tested by a pH meter (HI 2020F edge, Hanna Instruments) and tuned by adding 0.1 M NaOH. The stretching test was performed on electrodes with three passes of printing using a motorized force test stand (ESM303, Mark-10) with a speed of 10 mm/min. The speed of cyclic stretching is 20 mm/min. The SEM characterization was performed on JEOL 7600, and the surface conductivity of the electrode was tested by C-AFM (Asylum Research Cypher S). The XRD and XPS were characterized by a Shimadzu powder diffractometer (Cu Kα, λ = 1.5406 Å) and a Physical Electronics Inc. Quantera II, respectively. The FTIR spectrometer (Frontier, PerkinElmer) and the TG Q500 analyzer (TA Instruments) were used to characterize the functional groups and weight % of surfactant on Ag flakes, respectively.

The printing of stretchable Zn-Ag_2O sweat battery

The Zn flake powder and Ag_2O powder were mixed with carbon black (CB) at the weight ratios of 90:10 and 95:5, respectively, by mortar grinding for 10 min. The Zn inks and Ag_2O inks were formulated by mixing Zn/CB and Ag_2O/CB with the HPUA binder with the ratio of 1:2 and 1:1.2, respectively, and then shaking for 10 min. Two formulated inks were printed on the textile substrate in an interdigit shape in a laboratory-made black box and cured outside for 10 min without any heating or specific UV lightning. Then, Ag-HPUA inks were printed on top of two electrodes as the current collector and cured at the laboratory ambient environment.

The electrochemical characterization of stretchable Zn-Ag_2O sweat battery

The artificial sweats with a pH 4 with different NaCl/KCl concentrations were used as the electrolytes for in vivo studies. The polarization curves were tested by an electrochemical potentiostat (Autolab) with a scan rate of 5 mV/s from open circuit potential to 0 V. The discharging curve was obtained from a battery-testing instrument (Newar) at a current density of 0.2 mA/cm^2. The in vivo energy generation was tested by anchoring the printed battery with a series-connected 1-kilohm resistor on a subject's arm and monitoring the current of the circuit continuously during stationary cycling. The application demonstration of the battery was performed by powering a wireless epidermal temperature sensor (MMC-T201-1, Miaomiaoce, China) with a 5.6-mF capacitor to modulate the energy generated by four series-connected sweat batteries on the subject's arm. The voltage of the capacitor was measured by the DAQ6510 multimeter, and the temperature sensor sends in vivo data continuously to the application in smartphone every 2 s.

SUPPLEMENTARY MATERIALS

Supplementary material for this article is available at http://advances.sciencemag.org/cgi/content/full/7/29/eabg8433/DC1

REFERENCES AND NOTES

1. J. Xiong, J. Chen, P. S. Lee, Functional fibers and fabrics for soft robotics, wearables, and human-robot interface. *Adv. Mater.* **33**, 2002640 (2021).
2. T. R. Ray, J. Choi, A. J. Bandodkar, S. Krishnan, P. Gutruf, L. Tian, R. Ghaffari, J. A. Rogers, Bio-integrated wearable systems: A comprehensive review. *Chem. Rev.* **119**, 5461–5533 (2019).
3. T. Someya, Z. Bao, G. G. Malliaras, The rise of plastic bioelectronics. *Nature* **540**, 379–385 (2016).
4. W. Gao, S. Emaminejad, H. Y. Y. Nyein, S. Challa, K. Chen, A. Peck, H. M. Fahad, H. Ota, H. Shiraki, D. Kiriya, D.-H. Lien, G. A. Brooks, R. W. Davis, A. Javey, Fully integrated wearable sensor arrays for multiplexed in situ perspiration analysis. *Nature* **529**, 509–514 (2016).
5. Y. Ling, T. An, L. W. Yap, B. Zhu, S. Gong, W. Cheng, Disruptive, soft, wearable sensors. *Adv. Mater.* **32**, e1904664 (2020).
6. P. Li, Y. Zhang, Z. Zheng, Polymer-assisted metal deposition (PAMD) for flexible and wearable electronics: Principle, materials, printing, and devices. *Adv. Mater.* **31**, 1902987 (2019).
7. S. An, H. S. Jo, D.-Y. Kim, H. J. Lee, B.-K. Ju, S. S. Al-Deyab, J.-H. Ahn, Y. Qin, M. T. Swihart, A. L. Yarin, S. S. Yoon, Self-junctioned copper nanofiber transparent flexible conducting film via electrospinning and electroplating. *Adv. Mater.* **28**, 7149–7154 (2016).
8. J. Kim, A. S. Campbell, B. E.-F. de Ávila, J. Wang, Wearable biosensors for healthcare monitoring. *Nat. Biotechnol.* **37**, 389–406 (2019).
9. J. Wang, M.-F. Lin, S. Park, P. S. Lee, Deformable conductors for human-machine interface. *Mater. Today* **21**, 508–526 (2018).
10. H. Lee, C. Song, S. Baik, D. Kim, T. Hyeon, D.-H. Kim, Device-assisted transdermal drug delivery. *Adv. Drug Deliv. Rev.* **127**, 35–45 (2018).
11. X. Pu, W. Hu, Z. L. Wang, Toward wearable self-charging power systems: The integration of energy-harvesting and storage devices. *Small* **14**, 1702817 (2018).
12. J. Xiong, P. S. Lee, Progress on wearable triboelectric nanogenerators in shapes of fiber, yarn, and textile. *Sci. Technol. Adv. Mater.* **20**, 837–857 (2019).

13. J. Kim, I. Jeerapan, J. R. Sempionatto, A. Barfidokht, R. K. Mishra, A. S. Campbell, L. J. Hubble, J. Wang, Wearable bioelectronics: Enzyme-based body-worn electronic devices. *Acc. Chem. Res.* **51**, 2820–2828 (2018).
14. Y. Yu, H. Y. Y. Nyein, W. Gao, A. Javey, Flexible electrochemical bioelectronics: The rise of in situ bioanalysis. *Adv. Mater.* **32**, 1902083 (2020).
15. M. Bariya, H. Y. Y. Nyein, A. Javey, Wearable sweat sensors. *Nat. Electron.* **1**, 160–171 (2018).
16. J. Lv, I. Jeerapan, F. Tehrani, L. Yin, C. A. Silva-Lopez, J.-H. Jang, D. Joshuia, R. Shah, Y. Liang, L. Xie, F. Soto, C. Chen, E. Karshalev, C. Kong, Z. Yang, J. Wang, Sweat-based wearable energy harvesting-storage hybrid textile devices. *Energ. Environ. Sci.* **11**, 3431–3442 (2018).
17. Y. Yu, J. Nassar, C. Xu, J. Min, Y. Yang, A. Dai, R. Doshi, A. Huang, Y. Song, R. Gehlhar, A. D. Ames, W. Gao, Biofuel-powered soft electronic skin with multiplexed and wireless sensing for human-machine interfaces. *Sci. Robot.* **5**, eaaz7946 (2020).
18. L. Manjakkal, A. Pullanchiyodan, N. Yogeswaran, E. S. Hosseini, R. Dahiya, A wearable supercapacitor based on conductive PEDOT:PSS-coated cloth and a sweat electrolyte. *Adv. Mater.* **32**, 1907254 (2020).
19. A. J. Bandodkar, S. P. Lee, I. Huang, W. Li, S. Wang, C.-J. Su, W. J. Jeang, T. Hang, S. Mehta, N. Nyberg, P. Gutruf, J. Choi, J. Koo, J. T. Reeder, R. Tseng, R. Ghaffari, J. A. Rogers, Sweat-activated biocompatible batteries for epidermal electronic and microfluidic systems. *Nat. Electron.* **3**, 554–562 (2020).
20. H. Jin, N. Matsuhisa, S. Lee, M. Abbas, T. Yokota, T. Someya, Enhancing the performance of stretchable conductors for E-textiles by controlled ink permeation. *Adv. Mater.* **29**, 1605848 (2017).
21. L. Yin, J. Lv, J. Wang, Structural innovations in printed, flexible, and stretchable electronics. *Adv. Mater. Technol.* **5**, 2000694 (2020).
22. A. Kamyshny, S. Magdassi, Conductive nanomaterials for 2D and 3D printed flexible electronics. *Chem. Soc. Rev.* **48**, 1712–1740 (2019).
23. W. Zhou, S. Yao, H. Wang, Q. Du, Y. Ma, Y. Zhu, Gas-permeable, ultrathin, stretchable epidermal electronics with porous electrodes. *ACS Nano* **14**, 5798–5805 (2020).
24. N. Matsuhisa, D. Inoue, P. Zalar, H. Jin, Y. Matsuba, A. Itoh, T. Yokota, D. Hashizume, T. Someya, Printable elastic conductors by in situ formation of silver nanoparticles from silver flakes. *Nat. Mater.* **16**, 834–840 (2017).
25. D. Lu, C. P. Wong, Characterization of silver flake lubricants. *J. Therm. Anal. and Calorim.* **59**, 729–740 (2000).
26. A. Mena-Bravo, M. D. Luque de Castro, Sweat: A sample with limited present applications and promising future in metabolomics. *J. Pharm. Biomed. Anal.* **90**, 139–147 (2014).
27. S. Sun, Z. Pan, W. Zhang, F. K. Yang, Y. Huang, B. Zhao, Acid treatment of silver flake coatings and its application in the flexible electrical circuits. *J. Mater. Sci. Mater. Electron.* **27**, 4363–4371 (2016).
28. M. Grouchko, A. Kamyshny, C. F. Mihailescu, D. F. Anghel, S. Magdassi, Conductive inks with a "built-In" mechanism that enables sintering at room temperature. *ACS Nano* **5**, 3354–3359 (2011).
29. K. Parida, G. Thangavel, G. Cai, X. Zhou, S. Park, J. Xiong, P. S. Lee, Extremely stretchable and self-healing conductor based on thermoplastic elastomer for all-three-dimensional printed triboelectric nanogenerator. *Nat. Commun.* **10**, 2158 (2019).
30. D. Kokkinis, M. Schaffner, A. R. Studart, Multimaterial magnetically assisted 3D printing of composite materials. *Nat. Commun.* **6**, 8643 (2015).
31. D. K. Patel, A. H. Sakhaei, M. Layani, B. Zhang, Q. Ge, S. Magdassi, Highly stretchable and UV curable elastomers for digital light processing based 3D printing. *Adv. Mater.* **29**, 1606000 (2017).
32. D. Fu, W. Pu, Z. Wang, X. Lu, S. Sun, C. Yu, H. Xia, A facile dynamic crosslinked healable poly(oxime-urethane) elastomer with high elastic recovery and recyclability. *J. Mater. Chem. A* **6**, 18154–18164 (2018).
33. J. Xiong, G. Thangavel, J. Wang, X. Zhou, P. S. Lee, Self-healable sticky porous elastomer for gas-solid interacted power generation. *Sci. Adv.* **6**, eabb4246 (2020).
34. S.-M. Kim, H. Jeon, S.-H. Shin, S.-A. Park, J. Jegal, S. Y. Hwang, D. X. Oh, J. Park, Superior toughness and fast self-healing at room temperature engineered by transparent elastomers. *Adv. Mater.* **30**, 1705145 (2018).
35. Y. S. Choi, Y.-Y. Hsueh, J. Koo, Q. Yang, R. Avila, B. Hu, Z. Xie, G. Lee, Z. Ning, C. Liu, Y. Xu, Y. J. Lee, W. Zhao, J. Fang, Y. Deng, S. M. Lee, A. Vázquez-Guardado, I. Stepien, Y. Yan, J. W. Song, C. Haney, Y. S. Oh, W. Liu, H.-J. Yoon, A. Banks, M. R. MacEwan, G. A. Ameer, W. Z. Ray, Y. Huang, T. Xie, C. K. Franz, S. Li, J. A. Rogers, Stretchable, dynamic covalent polymers for soft, long-lived bioresorbable electronic stimulators designed to facilitate neuromuscular regeneration. *Nat. Commun.* **11**, 5990 (2020).
36. W. H. Lu, W. J. Xu, Y. M. Wu, X. Zhou, Y. B. Lu, Y. Q. Xiong, Synthesis of dendritic poly(urethane acrylate) used for UV-curable coatings. *Prog. Org. Coat.* **56**, 252–255 (2006).
37. I. You, M. Kong, U. Jeong, Block copolymer elastomers for stretchable electronics. *Acc. Chem. Res.* **52**, 63–72 (2019).
38. C. A. Silva, J. Lv, L. Yin, I. Jeerapan, G. Innocenzi, F. Soto, Y.-G. Ha, J. Wang, Liquid metal based island-bridge architectures for all Printed stretchable electrochemical devices. *Adv. Funct. Mater.* **30**, 2002041 (2020).
39. M. Zhang, R. Guo, K. Chen, Y. Wang, J. Niu, Y. Guo, Y. Zhang, Z. Yin, K. Xia, B. Zhou, H. Wang, W. He, J. Liu, M. Sitti, Y. Zhang, Microribbons composed of directionally self-assembled nanoflakes as highly stretchable ionic neural electrodes. *Proc. Natl. Acad. Sci. U.S.A.* **117**, 14667–14675 (2020).
40. J. Kim, R. Kumar, A. J. Bandodkar, J. Wang, Advanced materials for printed wearable electrochemical devices: A review. *Adv. Electron. Mater.* **3**, 1600260 (2017).
41. H. M. Emrich, E. Stoll, B. Friolet, J. P. Colombo, R. Richterich, E. Rossi, Sweat composition in relation to rate of sweating in patients with cystic fibrosis of the pancreas. *Pediatr. Res.* **2**, 464–478 (1968).
42. G. Liu, C. Ho, N. Slappey, Z. Zhou, S. E. Snelgrove, M. Brown, A. Grabinski, X. Guo, Y. Chen, K. Miller, J. Edwards, T. Kaya, A wearable conductivity sensor for wireless real-time sweat monitoring. *Sens. Actuators B* **227**, 35–42 (2016).
43. F. Herrmann, L. Mandol, Studies of pH of sweat produced by different forms of stimulation. *J.. Invest. Dermatol.* **24**, 225–246 (1955).
44. S. J. Lee, Y.-H. Kim, J. K. Kim, H. Baik, J. H. Park, J. Lee, J. Nam, J. H. Park, T.-W. Lee, G.-R. Yi, J. H. Cho, A roll-to-roll welding process for planarized silver nanowire electrodes. *Nanoscale* **6**, 11828–11834 (2014).
45. Y. Li, K.-s. Moon, H. Li, C. P. Wong, Development of isotropic conductive adhesives with improved conductivity, in *2004 Proceedings of the 9th International Symposium on Advanced Packaging Materials: Processes, Properties and Interfaces* (IEEE catalog no. 04TH8742, 2004), pp. 1–6.
46. D. Lu, Q. K. Tong, C. P. Wong, A study of lubricants on silver flakes for microelectronics conductive adhesives. *IEEE Trans. Compon. Packaging Technol.* **22**, 365–371 (1999).
47. F. Tan, X. Qiao, J. Chen, Removal of chemisorbed lubricant on the surface of silver flakes by chemicals. *Appl. Surf. Sci.* **253**, 703–707 (2006).
48. X. Li, J. J. Lenhart, H. W. Walker, Dissolution-accompanied aggregation kinetics of silver nanoparticles. *Langmuir* **26**, 16690–16698 (2010).
49. T. S. Peretyazhko, Q. Zhang, V. L. Colvin, Size-controlled dissolution of silver nanoparticles at neutral and acidic pH conditions: Kinetics and size changes. *Environ. Sci. Technol.* **48**, 11954–11961 (2014).
50. C. Levard, S. Mitra, T. Yang, A. D. Jew, A. R. Badireddy, G. V. Lowry, G. E. Brown Jr., Effect of chloride on the dissolution rate of silver nanoparticles and toxicity to *E. coli*. *Environ. Sci. Technol.* **47**, 5738–5745 (2013).
51. Y. Li, J. Zhao, E. Shang, X. Xia, J. Niu, J. Crittenden, Effects of chloride ions on dissolution, ROS generation, and toxicity of silver nanoparticles under UV irradiation. *Environ. Sci. Technol.* **52**, 4842–4849 (2018).
52. M. El, F. Nehal, A. Bouzidi, A. Nakrela, R. Miloua, M. Medles, R. Desfeux, J.-F. Blach, P. Simon, M. Huvé, Synthesis and characterization of antireflective Ag@AgCl nanocomposite thin films. *Optik* **224**, 165568 (2020).
53. K. I. Peterson, M. E. Lipnick, L. A. Mejia, D. P. Pullman, Temperature dependence and mechanism of chloride-Induced aggregation of silver nanoparticles. *J. Phys. Chem. C* **120**, 23268–23275 (2016).
54. Y.-X. Zeng, X.-W. Zhong, Z.-Q. Liu, S. Chen, N. Li, Preparation and enhancement of thermal conductivity of heat transfer oil-based MoS_2 nanofluids. *J. Nanomater.* **2013**, 270490 (2013).
55. L. Wang, X. Fu, J. He, X. Shi, T. Chen, P. Chen, B. Wang, H. Peng, Application challenges in fiber and textile electronics. *Adv. Mater.* **32**, 1901971 (2020).
56. N. von Goetz, C. Lorenz, L. Windler, B. Nowack, M. Heuberger, K. Hungerbühler, Migration of Ag- and TiO_2-(Nano)particles from textiles into artificial sweat under physical stress: Experiments and exposure modeling. *Environ. Sci. Technol.* **47**, 9979–9987 (2013).
57. D. G. Mackanic, X. Yan, Q. Zhang, N. Matsuhisa, Z. Yu, Y. Jiang, T. Manika, J. Lopez, H. Yan, K. Liu, X. Chen, Y. Cui, Z. Bao, Decoupling of mechanical properties and ionic conductivity in supramolecular lithium ion conductors. *Nat. Commun.* **10**, 5384 (2019).
58. D. R. Seshadri, E. V. Davies, E. R. Harlow, J. J. Hsu, S. C. Knighton, T. A. Walker, J. E. Voos, C. K. Drummond, Wearable sensors for COVID-19: A call to action to harness our digital infrastructure for remote patient monitoring and virtual assessments. *Front. Digit. Health* **2**, 8 (2020).

Acknowledgments

Funding: The project is funded by the National Research Foundation under the NRF-Investigatorship NRF-NRFI2016-05. **Author contributions:** J.L., G.T., and P.S.L. conceived the idea, designed the experiments, guided the projects, and wrote the manuscript. G.T. performed the synthesis, characterizations, and analysis of elastomer. J.L., Y.L., D.G., and J.Ch. formulated Ag-HPUA inks and performed the characterizations, applications, and analysis of the electrodes and devices. J.X. performed SEM characterization, result discussion, and on-body experiments. J.Ci., M.W.M.T., I.A., and S.C. contributed to chemical bonds characterization, thermal analysis, AFM characterization, and XRD analysis, respectively. X.Z.

and W.C.P. assisted in direct writing and NMR characterization, respectively. J.L. and G.T. contributed equally to this work. P.S.L. supervised this project. All authors discussed the results and commented on the manuscript. **Competing interests:** J.L., G.T., and P.S.L. are the inventor for "Conductive electronic textiles" filed by the Nanyang Technological University (Singapore provisional patent application no. 10202100851 U). The authors declare that they have no other competing interests. **Data and materials availability:** All data needed to evaluate the conclusions in the paper are present in the paper and/or the Supplementary Materials. Additional data related to this paper may be requested from the authors.

Submitted 1 February 2021
Accepted 28 May 2021
Published 14 July 2021
10.1126/sciadv.abg8433

Citation: J. Lv, G. Thangavel, Y. Li, J. Xiong, D. Gao, J. Ciou, M. W. M. Tan, I. Aziz, S. Chen, J. Chen, X. Zhou, W. C. Poh, P. S. Lee, Printable elastomeric electrodes with sweat-enhanced conductivity for wearables. *Sci. Adv.* **7**, eabg8433 (2021).